Josephson Detection of Time Reversal Symmetry Breaking $s \pm is'$ Superconductivity in SnTe Nanowires

C. J. Trimble,[1†] M. T. Wei,[1†] N. F. Q. Yuan,[2] S. S. Kalantre,[1]
P. Liu,[3,4] J. J. Cha,[3,4,5] L. Fu,[2] J. R. Williams[1*]

[1] *Joint Quantum Institute and Center for Nanophysics and Advanced Materials Department of Physics, University of Maryland, College Park, MD USA*
[2] *Department of Physics, Massachusetts Institute of Technology, Cambridge, MA USA*
[3] *Department of Mechanical Engineering and Materials Science, Yale University New Haven, CT, USA*
[4] *Energy Sciences Institute, Yale West Campus, West Haven, CT, USA*
[5] *Canadian Institute for Advanced Research Azrieli Global Scholar, Toronto, ON, Canada*
[†] *These authors equally contributed.*
[*] *To whom correspondence should be addressed; E-mail: jwilliams@physics.umd.edu.*

(Dated: July 10, 2019)

Exotic superconductivity, such as high T_C, topological, and heavy-fermion superconductors, often rely on phase sensitive measurements to determine the underlying pairing. Here we investigate the proximity-induced superconductivity in nanowires of SnTe, where a $s \pm is'$ superconducting state is produced that lacks the time-reversal and valley-exchange symmetry of the parent SnTe. A systematic breakdown of three conventional characteristics of Josephson junctions – the DC Josephson effect, the AC Josephson effect, and the magnetic diffraction pattern – fabricated from SnTe nanowire weak links elucidates this novel superconducting state. Further, the AC Josephson effect reveals evidence of a Majorana bound state, tuned by a perpendicular magnetic field. This work represents the definitive phase-sensitive measurement of novel $s \pm is'$ superconductivity, providing a new route to the investigation of fractional vortices, topological superconductivity, topological phase transitions, and new types of Josephson-based devices.

The nature of paired electrons in solid material remains one of the most important areas of research in condensed matter physics. Beyond the framework of conventional (BCS) superconductors, pairing can arise in materials with a multitude of mechanisms for coupling two electrons, which can results in a variety of gap symmetries [1]. In the classification of these superconductors, determination of phase of the superconducting order parameter is of paramount importance. This is also evident in materials with the requisite criterion for topological phases of matter, where the determination of the sign of the order parameter is essential in uncovering the nontrivial topologies in the superconducting state [2].

Most conventional descriptions of superconductors detail the effects of pairing within a single electronic band. Yet, adding another superconducting component – for example, superconductivity arising on a second electronic band – can augment the available ground states [3–5]. One possibility is the occurrence of a sign change (i.e. a phase angle of π) between superconducting order parameters on two different bands: a so called $s\pm$ superconductor. Such an effect is thought to be prevalent in Fe-based superconductors, and experiments have begun to observe signatures consistent this state [6–8]. However, this effect has yet to be seen outside of Fe-based materials and conclusive evidence of this exotic superconducting state has remained elusive. SnTe, a topological crystalline insulator [9], has an even number of Dirac valleys [10]. In this work, the presence of two bands dramatically alters the observed behavior of Josephson junctions (JJs) fabricated using SnTe nanowires as a weak link. This provides clear evidence of proximity-induced $s \pm is'$ superconducting state, a relative of an $s\pm$ state but with an angle in phase between the bands that is neither zero nor π, as detailed below.

Upon placing an s-wave superconductor in proximity to SnTe (Fig. 1A), superconducting order will be induced in each of the two bands in SnTe. To allow interactions between bands, a momentum-conserving interband Umklapp scattering process is included [11]. The phase-dependent part of the free energy derived is of the form

$$F(\theta_1, \theta_2) = J\cos(\theta_1 - \theta_2) + J'(\cos\theta_1 + \cos\theta_2) \qquad (1)$$

where $\theta_{j=1,2}$ are the phases of the superconducting order parameter in each band, J is a measure of the interband coupling (provided by Umklapp process) and J' a measure of the external pairing field (provide by the Al superconducting leads). Minimization of this free energy dictates that the ground state is given by the condition $\theta_1 = -\theta_2$, with a built in phase difference between bands $\theta \equiv \theta_1 - \theta_2$ given by

$$\theta = 2\mathrm{Re}(\arccos(\delta/2)), \quad \delta = |\frac{J'}{J}|. \qquad (2)$$

The result of the above formulation is a built-in pairing phase difference between two bands which is possible for values of $\delta \leq 2$ (Fig. 1E). If a finite phase difference between bands occurs, the superconducting order parameter for the material becomes $s \pm is'$: one pocket has an

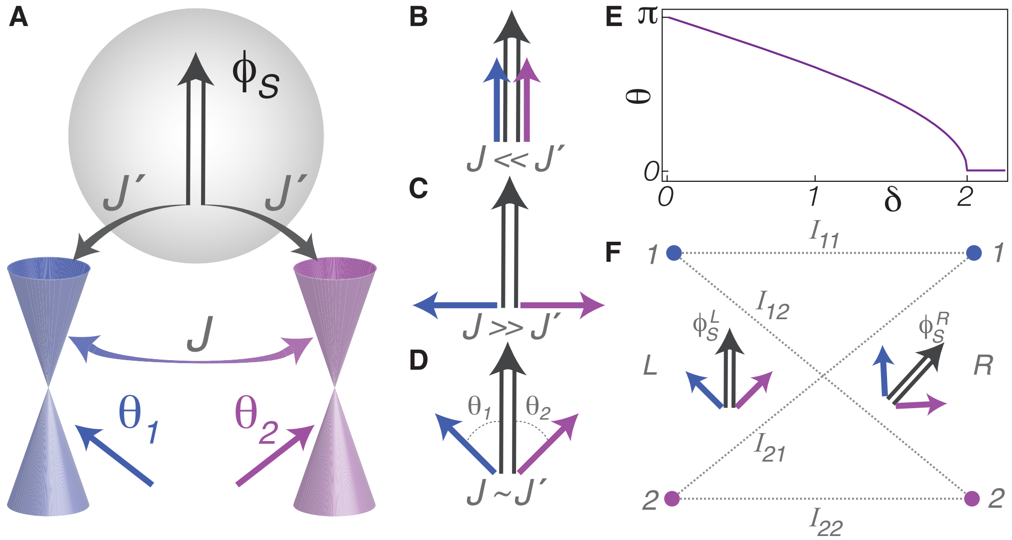

FIG. 1: **Induced $s \pm is'$ superconductivity in SnTe.** (**A**) The two bands in SnTe are coupled to the order parameter ϕ_S in aluminum via an external pairing field J'. The interband coupling J is facilitated via the Umklapp process. θ_1 and θ_2 are the phases of individual order parameters in the two bands. (**B**)-(**D**) The competition between the coupling strengths J and J' results in different relative phases between two bands: (**B**) When $J \ll J'$, the phases tend to align with each other. (**C**) When $J \gg J'$, the phases of two bands are out of phase by π. (**D**) In the intermediate regime $J \sim J'$, the phases are canted. (**E**) The phase difference between two bands $\theta \equiv \theta_1 - \theta_2$ as a function of the coupling strength ratio $\delta = J'/J$ given by Eq. (2). The nonzero canting angle yields the $s \pm is'$ superconductivity in SnTe. (**F**) The four-channel supercurrent flow between two superconducting electrodes L and R. The two intraband channels I_{ii} behave like conventional "0"-junctions, while the interband channels are negatively coupled and thus behave like "π"-junctions. The total supercurrent is governed by the phase difference between two conventional superconductors $\phi = \phi_s^R - \phi_s^L$, resulting in a relative rotation that changes the relative amount of supercurrent contributed by each channel.

order parameter $\Delta_1 + i\Delta_2$, the other $\Delta_1 - i\Delta_2$, where $\Delta_{j=1,2}$.

The free energy above is distinct from the conventional free energy of Josephson junctions. In the ground state, both time-reversal symmetry ($\theta_j \to -\theta_j$) and valley-exchange symmetry $\theta_1 \leftrightarrow \theta_2$ resulting from the four-fold rotational symmetry – two symmetries which were preserved prior to inducing superconductivity – are broken, while their product ($\theta_i \to -\theta_j$) is preserved. Further, the criterion that $\theta_1 = -\theta_2$ results in a free energy with two minima per period, distinct from the single minimum of conventional junctions [12]. Finally, the competition between J and J' should be noted: J' tends to want to align the superconducting phases of both bands, whereas J acts to drive the phases to be shifted by π. This competition leads to three configurations of the relative phases (Fig. 1B-D).

The resulting Josephson effects are influenced by the competition described above. Theoretical investigations of time reversal symmetry breaking (TRSB) have been explored in junctions and interfaces between $s\pm$ and s-wave superconductors [5, 13, 14]. The manifestation of TRSB is two-fold. First is the creation of a canted state (Fig. 1D) [13–16], where a nonzero angle forms between phase of the bands and the phase of the superconductor ϕ_S. This canting is similar in nature to the state generated when antiferromagnetic spins are placed in a magnetic field. The resulting effect of this canting is the generation of chiral currents in momentum space [13, 14] – a clear indication of time reversal symmetry breaking. A graph of the canting angle $\theta = \theta_1 - \theta_2$ calculated from Eq. 3 is shown in Fig. 1E. Concurrent with the transition to the canted state is the generation of a predominant second harmonic in the current phase relation [16, 17].

The second result of TRSB is the presence of four channels of supercurrent flow (Fig. 1F) [5, 14]. Whereas the intraband contribution arises from two conventionally coupled channels represented by $I_{ii} = I_{ii}^C \sin(\theta_i^R - \theta_i^L)$ (where L and R are the angles on the left and right Al-SnTe interfaces), the interband channels are negatively coupled, producing two "π"-junction channels in the form $I_{ij} = -I_{ij}^C \sin(\theta_i^R - \theta_j^L)$ (where i, j=1,2 indicates the band and I_{ii}^C and I_{ij}^C are critical currents of the intra and interband supercurrent respectively). The total supercurrent is governed by the phases of the two conventional superconductors ($\phi_s^R - \phi_s^L$): a nonzero supercurrent will produce a relative rotation $\phi = \phi_s^R - \phi_s^L$ (Fig. 1F), thus altering each channel's relative contribution to the total supercurrent.

Below we detail the manner in which three characteristic properties of SnTe Josephson junctions (JJs) are affected in a consistent with the above formulation. These three characteristics are the following: the DC Josephson effect, by which a superconducting-to-normal transition is driven by an external DC current; the AC Josephson effect, whereby application of radio-frequency radiation produces frequency-dependent steps in the current versus voltage curves; and the magnetic diffraction pattern, an effect where a magnetic field applied perpendicular to the junction modulates the measured critical current I_C. The behavior of each of these relies on the current-phase relation (CPR) ($I_S(\phi) = dF/d\phi$); hence, it is expected that the anomalous free energy derived above will produce modified junction behavior. We also find that the effect is most prominent in the nanowires with the smallest diameter [11], suggesting that topological surface state plays an important role in the observations [18].

The Josephson effect of aluminum/SnTe nanowire/aluminum JJs is measured by a lock-in detection of the differential resistance $r = dV/dI$ as a function of the applied DC current (I_{DC}), perpendicular magnetic field (B) and AC current (measured in power P). $r(I_{DC})$ at $B, P = 0$ is shown in Fig. 2A. Unlike conventional overdamped JJs, different values of I_C are observed for positive (I_C^+) and negative (I_C^-) values of I_{DC}. We note that in underdamped junctions, different values for I_C can be observed, which reflect the difference in switching and retrapping currents and produce a hysteric $I - V$ curve [12]. However, as shown in Fig. 2A, sweeps of I_{DC} in both directions reveal that the difference in I_C^+ and I_C^- remains intrinsically and no hysteresis is observed, ruling out this phenomenon. A current-direction-dependent I_C has also been observed in so-called "ϕ_0" junctions [19–21], giving the first indication that a similar phenomenon is observed here.

To understand the origin of the difference between I_C^+ and I_C^-, numerical simulations of the resistively-shunted junction model [11]) were performed. Conventional JJs possess a CPR which is both inversion and π-translation symmetric, a result of time-reversal symmetry and insensitivity to changes of ϕ by 2π. The only way to reproduce $r(I_{DC})$ curves that are not symmetric in I_{DC} is to break both of these symmetries, resulting in a CPR of the form $I_S = \sin(\phi + \beta) + A\sin(2\phi + \beta)$, where β is fit parameter and $A = 0.909$ is determined by the AC Josephson effect. This inclusion of a second harmonic is expected in the TRSB state and will be confirmed in our measurement of the AC Josephson effect (Fig. 4). Values of $\beta = (-0.84, -0.08)\pi$ best match the experimental data, producing the CPRs shown in Fig. 2C. Most surprising about the CPR shown in Fig. 2C is the nonzero supercurrent which exist for $\phi = 0$, a clear signature of TRSB and the existence of a ϕ_0-junction.

The generation of a ϕ_0-junction from the four supercurrents of Fig. 1F is surprising. π-junction effects have been predicted in $s\pm$ junctions [17, 22–25]. However, a lateral (along the direction perpendicular to current flow) variation of the predominance of either a "0" or "π" supercurrent or a variation of interband coupling is required to produce a ϕ_0-junction. In the absence of these effects, the expected result of this coexistence is a reduction of the critical current since 0 and π channels spatially coexist [14, 23]. Calculations of the CPR in coupled canted phase junctions where all band angles are equal ($\theta_1^L = \theta_2^L = \theta_1^R = \theta_2^R$, where are angles are referenced to ϕ_S^L, taken to be zero) confirms this result [11]. While it may be possible that the relative strength of the 0 and π channels or the coupling varies laterally, we do not know of a reason for this variation in our devices.

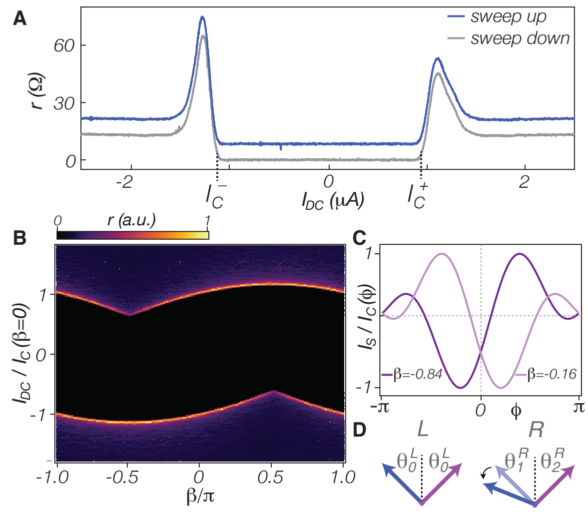

FIG. 2: **Breakdown of the DC Josephson Effect.** (**A**) Differential resistance r as a function of DC bias current I_{DC} in different sweep directions. The bias sweeps show no hysteresis and two nonidentical critical currents I_C^+ and I_C^-. The curves are offset for clarity. (**B**) The simulated differential resistance $r(I_{DC}, \beta)$ calculated by the resistively-shunted junction model using a CPR of $I_S = \sin(\phi + \beta) + A\sin(2\phi + \beta)$, where the best fit parameters β with the experiment are -0.84π and -0.16π. The resulting CPRs are plotted in (**C**). Both CPRs show nonzero supercurrent for $\phi = 0$, giving robust evidence of TRSB and the existence of a ϕ_0-junction. (**D**) In the canted phase picture, a slight difference in the angle θ_1^R from the opposite band is essential to the formation of the ϕ_0-junction.

However, a simple modification canted-phase junction can allow for the formation of a ϕ-junction: allowing θ_1^R to be different from the other band angles (Fig. 2D). This may arise either from an inhomogeneous coupling between the two bands of SnTe and the superconductor [15] or from the presence of the interband current arising in the TRSB state [13, 14]. The resulting intra- and interband CPRs are

$$\begin{aligned}
I_{ii}(\phi) &= I_{ii}^C\{[\sin(\theta_1^R - \theta_0^L) + \sin(\theta_0^L - \theta_2^R)]\cos\phi \\
&+ [\cos(\theta_1^R - \theta_0^L) + \cos(\theta_0^L - \theta_2^R)]\sin\phi\}, \\
I_{ij}(\phi) &= -I_{ij}^C\{[\sin(\theta_1^R + \theta_0^L) - \sin(\theta_0^L + \theta_2^R)]\cos\phi \\
&+ [\cos(\theta_1^R + \theta_0^L) + \cos(\theta_0^L + \theta_2^R)]\sin\phi\}.
\end{aligned} \tag{3}$$

Here we have taken the two angles on the left side of the junction to be equal and opposite with value θ_0^L and allowed the angles on the right (θ_1^R, θ_2^R) to vary. Similar results are obtained if the angles on the left are also allowed to vary. The key feature of this result is the

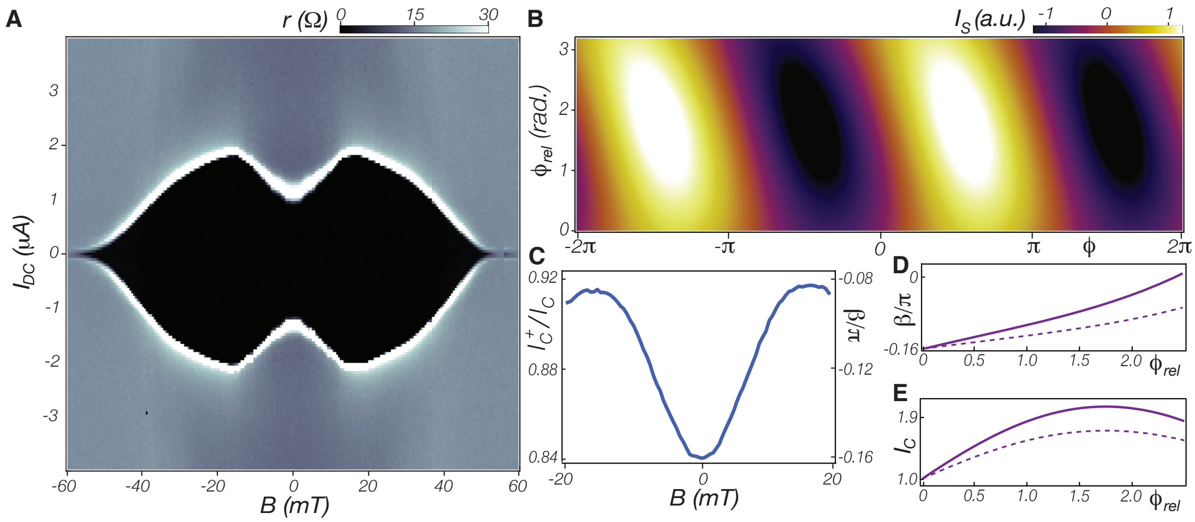

FIG. 3: **The Anomalous Magnetic Diffraction Pattern.** (**A**) Plot of $r(B, I_{\rm DC})$ taken at 25 mK which shows a characteristic minimum in $I_{\rm C}$ at B=0. (**B**) Calculated CPRs as ϕ_{rel} is cycled. (**C**) The ratio of I_C^+ to I_C^- as a function of B, shown between -20 and 20 mT where the Al leads are unaffected by B. (**D-E**) the variation in fit parameter β (**D**) and critical current (**E**) as ϕ_{rel} is cycled. The dashed line in D, E are running averages.

presence of both a $\cos\phi$ and a $\sin\phi$ term, which allow for nonzero supercurrent at ϕ=0.

The anomalous CPR extracted from the DC Josephson effect should also change the behavior of two other JJ characteristics –the magnetic diffraction pattern (MDP) and the AC Josephson effect. The magnetic diffraction pattern ($r(I_{DC}, B)$) is shown in Fig. 3, where B is applied perpendicular to the sample substrate. Unlike the MDPs of typical Josephson junctions [26], SnTe junctions display a local minimum of the critical current at zero magnetic field. The peak in I_C occurs at B=16mT which, when using the area of the junction (defined as the length of the junction plus twice the penetration depth), corresponds to a flux through the device of $\sim\ \Phi_0/4$ (where Φ_0 is the quantum of flux). This contrasts with the Fraunhofer-resembling patterns that have been observed in junctions with weak links of bulk TCIs [27], topological insulators [28–30], and strong-spin-orbit 1D wires [31], where a maximum in I_C at B=0 is still observed. Measurements in a parallel field do not produce this effect [11], ruling out spin-orbit or phase-coherent effects being the origin of the rise in I_C away from $B = 0$.

A minimum in I_C has also been observed in other JJs, like in high-T$_C$ corner junctions [32] and S-ferromagnet-S JJs [33], each of which also has two supercurrent components that are shifted in phase. Again, this result relies on a lateral variation of the relative strengths of 0 and π channels. These junctions also have a maximum in I_C at a flux of Φ_0. Anomalous Fraunhofer patterns have been predicted in $s\pm$ corner junctions with a 135^o angle [34]. Since neither of these seem to match our experiment, we again turn to Eq. 4 to find an origin for this effect.

Application of a perpendicular magnetic field produces a nonzero Aharonov-Bohm phase in the lateral direction, causing a relative rotation ϕ_{rel} of the local phase between the left and right superconductors forming the junction. This relative phase also adjusts the angles θ_1^R and θ_2^R in Eq. 4. Shown in Fig. 3B are the calculated CPRs as ϕ_{rel} changes from 0 to π. These calculations were performed using angles $\theta_0^L = \theta_2^R = \pi/22$ and $\theta_1^R = \pi/1.7$; similar behavior is observed for a wide range of parameters, although these do not quantitatively match the experimental observations [11]. It is observed that both I_C and β are changed as ϕ_{rel} changes. Between ϕ_{rel}=0 and ϕ_{rel}=$\pi/2$ (the expected shift for $\Phi_0/4$), β changes from -0.16π to -0.04 and I_C is increased by a factor of 1.9. This closely matches the observed behavior in experiment for I_C (Fig. 3A) and β (Fig. 3C). For this comparison, we note that the β and I_C extract from simulation are a local values whereas, experiment measures the global value (i.e. average across the entire device). Hence, the running averages of Fig. 3D, E (dashed lines) should be compared to experiment. The results of Fig. C are only shown between $\pm$20mT, after which the Al leads are affected by B, complicating comparison to simulation. Finally, we mention that we also observe a 0 to π transition as a function of ϕ_{rel} for certain parameter ranges [11]. This is an alternate explanation for the observe increase in $I_C(B)$.

We now turn our attention to the modification of the AC Josephson effect. The presence of a second harmonic component – expected in the TRSB state [16, 17] – will result in additional steps at values of half the expected $hf/2e$. A plot of $r(I_{DC}, P), B = 0$ is shown in Fig. 4A (grey curve) taken at f =5 GHz, where dips in r are observed at both integer and half-integer values. This is more clearly seen in the integrated voltage $V = \int (dV/dI) dI$ versus I_{DC} curve shown in blue.

The dips/plateaus measured are of nearly equal strength, indicating that the contribution of the first and second harmonic to the CPR are approximately equal. Subharmonic steps are expected for underdamped junctions and for overdamped junctions with a skewed CPR. Our junctions are overdamped; hence we rule out the former as being the cause. Skewed CPRs in overdamped junctions produce fractional Shapiro steps, but the strength of these steps is much reduced compared to the integer steps (see Ref. [27] for comparison if the AC Josephson effect with a skewed CPR in a similar material, $Pb_{0.5}Sn_{0.5}Te$). Therefore, we also rule out the skewed CPR as the source of the observed effect.

Application of a magnetic field influences the features observed in the AC Josephson effect. Fig. 3B shows a plot which resembles Fig. 3A, except that it was taken at $B = 16\,\mathrm{mT}$, the field at which I_C is a maximum. Here, the fractional steps appear more pronounced compared to $B = 0$. In fact, the subharmonic features are most intense at $B = 16$ mT and disappear entirely for $B > 30\mathrm{mT}$ [11].

As such, we analyze the magnetic field dependence of the AC Josephson effect (Fig. 4C). Most striking is the merging of the first and second step, which begins around B=8mT and persists until just past the field of maximum I_C. Merging of the first and second steps can arise from nonlinear, period-doubling effects, known from the study of junctions driven by AC voltages [35]. This seem unlikely for two reasons. First, the junctions under study are in the overdamped regime where chaotic effects are known to be absent. Second, the only parameter which is varied by the magnetic field is I_C. For values of B where I_C is the same, two different behaviors are observed: I_C=1.2μA both at B=8 and 28 mT, yet only at the lower field are the two steps merged. Note that Fig. 4C is taken at P=-20.0dBm; at these low powers the half steps are merged with the integer steps (see Ref. [11]).

Recently, it has been shown that junctions with a mixture of 2π and 4π CPRs arising from the presences of topologically trivial and nontrivial Andreev bound states can produce a disappearance of the first Shapiro step [36–38]. At B=8mT, $\phi_{rel} = \pi/4$, at which point band 1 on the right is π out of phase with band 2 on the left ($\theta_1^R - \theta_0^L \sim \pi$, see inset of Fig. 4C). Thus, at this point the 4π periodic CPR would contribute to the overall supercurrent and cause a merging of the first and second step. This effect persists until θ_1^R moves past being out of phase with band 1 on the left. This means that the conditions for a Majorana bound state are satisfied in this regime. This effect warrants further theoretical studies and current experimental investigations are underway.

Acknowledgments: This work was sponsored by the grants National Science Foundation A "Quantum Leap" Demonstration of Topological Quantum Computing (DMR-1743913) and Physics Frontier Center at the Joint Quantum Institute (PHY-1430094).

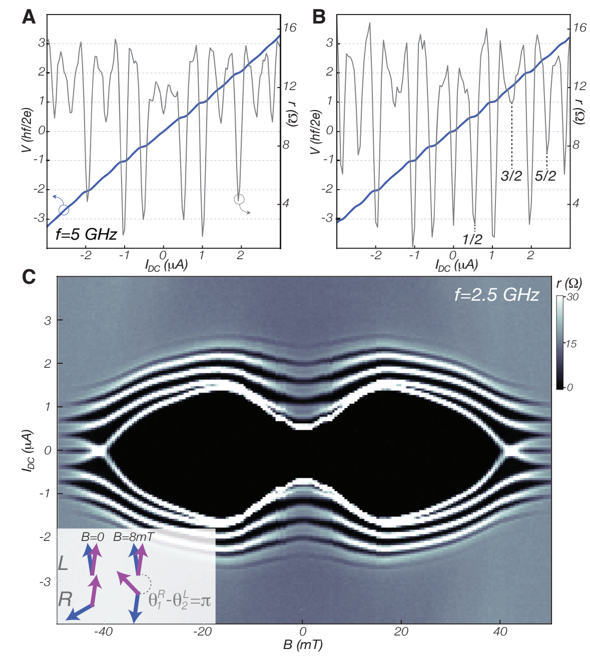

FIG. 4: **AC Josephson Effect.** (**A**) Fractional Shapiro steps appearing in a plot of $r(I_{\mathrm{DC}})$ (grey curve) and integrated voltage $V(I_{\mathrm{DC}})$ (blue curve) taken at an applied RF frequency $f = 5$ GHz, P = -11.8 dBm, and $B = 0$ mT. (**B**) A similar plot of $r(I_{\mathrm{DC}})$ and $V(I_{\mathrm{DC}})$, this time with an applied RF frequency $f = 5$ GHz, P = -8.0 dBm, and $B = 16$ mT. The fractional steps here deepen in comparison to the B=0 mT case. Plots (**A**) and (**B**) are intentionally collected at slightly different P to account for a shift in the step pattern brought about by changes in B [11]. (**C**) Plot of $r(B, I_{\mathrm{DC}})$ taken with f=2.5Ghz and P=-20.0 dBm which shows the B field dependence of the AC Josephson effect. Interestingly, the first Shapiro step disappears in the range B=8-20 mT, where the conditions for a Majorana bound state are met. Inset: Approximate angles θ_1^L and θ_1^R at B=0, 8 mT.

[1] A. J. Leggett, *Annu. Rev. Condens. Matter Phys.* **2**, 11 (2011).
[2] X.-L. Qi, T. L. Hughes, and S.-C. Zhang, *Phys. Rev. B* **81**, 134508 (2010).
[3] D. Pekker and C. M. Varma, *Ann. Rev . Condens. Matter Phys.* **6**, 267-297 (2015).
[4] Y. Tanaka, *Supercond. Sci. Technol.* **28** 034002 (2015).
[5] Y. Yerin, and A. N. Omelyanchouk, *Low Temp. Phys.* **43**, 1013 (2017).
[6] T. Hanaguri, S. Niitaka, K. Kuroki, H. Takagi, *Science* **328**, 474-476 (2010).
[7] C.-T. Chen *et al.*, *Nature Phys.* **6** 260-264 (2010).
[8] A. A. Kalenyuk *et al.*, *Phys. Rev. Lett.* **120**, 067001 (2018).
[9] L. Fu, *Phys. Rev. Lett.* **106**, 106802 (2011).
[10] T. H. Hsieh *et al.*, *Nature Comm.* **3**, 982 (2012).
[11] Details on the calculations and further experimental data will be available at the time of publication.
[12] M. Tinkham, *Introduction to Superconductivity*, Dover Publications, Second Edition (2004).
[13] T. K. Ng and N. Nagaosa, *EPL* **87**, 17003 (2009).
[14] S.-Z. Lin, *Phys. Rev. B* **86**, 014510 (2012).

[15] V. G. Stanev and A. E. Koshelev, *Phys. Rev. B* **86**, 174515 (2012).
[16] A. E. Koshelev, *Phys. Rev. B* **86**, 214502 (2012).
[17] E. Berg, N. H. Lindner, and T. Pereg-Barnea, *Phys. Rev. Lett.* **106**, 147003 (2011).
[18] P. Liu, J. R. Williams, J. J. Cha, *Nat. Rev. Mater.* **4**, 479 (2019).
[19] E. Goldobin, D. Koelle, R. Kleiner, and A. Buzdin, *Phys. Rev. B* **76**, 224523 (2007).
[20] E. Goldobin, D. Koelle, R. Kleiner, and R. G. Mints, *Phys. Rev. Lett.* **107**, 227001 (2011).
[21] H. Sickinger *et al.*, *Phys. Rev. Lett.* **109**, 107002 (2012).
[22] J. Linder, I. B. Sperstad, and A. Sudbø, *Phys. Rev. B* **80**, 020503 (2009).
[23] W. -Q. Chen and F. -C. Zhang, *Phys. Rev. B* **83**, 212501 (2009).
[24] Y. Ota, M. Machida, T. Koyama, and H. Matsumoto, *Phys. Rev. Lett.* **102**, 237003 (2009).
[25] W. -Q. Chen, F. Ma, Z. -Y. Lu, and F. -C. Zhang, *Phys. Rev. Lett.* **103**, 207001 (2009).
[26] A. Barone, G. Paternò, *Physics and Applications of the Josephson Effect.* (Wiley-Interscience Publications, Canada (1982).
[27] R. Snyder *et al.*, *Phys. Rev. Lett.* **121**, 097701 (2018).
[28] J. R. Williams *et al.*, *Phys. Rev. Lett.* **109**, 056803 (2012).
[29] M. Veldhorst *et al.*, *Nature Mat.* **11**, 417 (2012).
[30] S. Hart *et al.*, *Nature Phys.* **10**, 638-643 (2014).
[31] K. Zuo *et al.*, *Phys. Rev. Lett.* **119**, 187704 (2017).
[32] D. J. Van Harlingen, *Rev. Mod. Phys.* **67**, 515 (1995).
[33] M. Weides *et al.*, *Phys. Rev. Lett.* **97**, 247001 (2006).
[34] J. Wu and P. Phillips, *Phys. Rev. B* **79**, 092502 (2009).
[35] R. L. Kautz, *Rep. Prog. Phys.* **59** 935 (1996).
[36] J. Wiedenmann *et al.*, *Nature Comm.* **7**, 10303 (2016).
[37] J. Picó-Cortés, F. Domínguez, and G. Platero, *Phys. Rev. B* **96**, 125438 (2017).
[38] K. Le Calvez *et al.*, *Nature Comm. Phys.* **2**, 4 (2019).